# Entanglement Distribution in Satellite-based Dynamic Quantum Networks

Alena Chang, *Student Member*, *IEEE*, Yinxin Wan, *Member*, *IEEE*, Guoliang Xue, *Fellow*, *IEEE*, Arunabha Sen, *Senior Member*, *IEEE*

***Abstract*—Low Earth Orbit (LEO) satellites present a compelling opportunity for the establishment of a global quantum information network. However, satellite-based entanglement distribution from a networking perspective has not been fully investigated. Existing works often do not account for satellite movement over time when distributing entanglement and/or often do not permit entanglement distribution along inter-satellite links, which are two shortcomings we address in this paper. We first define a system model which considers both satellite movement over time and inter-satellite links. We next formulate the optimal entanglement distribution (`OED`) problem under this system model and show how to convert the `OED` problem in a dynamic physical network to one in a static logical graph which can be used to solve the `OED` problem in the dynamic physical network. We then propose a polynomial time greedy algorithm for computing satellite-assisted multi-hop entanglement paths. We also design an integer linear programming (ILP)-based algorithm to compute optimal solutions as a baseline to study the performance of our greedy algorithm. We present evaluation results to demonstrate the advantage of our model and algorithms.**

## 1. Introduction

Predicated entirely on entanglement, quantum networks enable Alice to securely send information to Bob by teleporting the state of a qubit from her site to that of Bob without physically transferring the qubit itself, consuming the entanglement in the process [14]. Entanglement is thus regarded as a precious resource in quantum communications, a currency dubbed *ebits*.

Repeaters in a quantum network employ local operations and classical communication (LOCC) to manipulate the state of one or more qubits in order to facilitate end-to-end entanglement between two parties who may not be directly connected by a physical communication link. We first generate entanglements between adjacent repeaters along links to form a repeater chain of entangled photon pairs between Alice and Bob. We then perform entanglement swapping [2] by applying a Bell state measurement (BSM) at each of the intermediate repeaters, transforming two consecutive entanglements into one, until Alice and Bob directly share an entangled photon pair. Alice and Bob may now use this ebit to perform quantum teleportation. The entire process is assisted by classical heralding signals which indicate whether an attempt at entanglement generation or entanglement swapping is successful.

Based on recent advances in space quantum communications [9, 13], satellites, particularly Low Earth Orbit (LEO) satellites, are poised to be essential vehicles for the establishment of a global quantum information network. Entanglement distribution in a space-ground scheme can be accomplished in different ways, which we describe in the following.

The scheme proposed in [1] describes a *double downlink configuration*, in which satellites armed with entanglement sources beam down entangled photon pairs to two ground repeater stations at a time. Each ground repeater houses a number of quantum non-demolition (QND) measurement devices and quantum memories (QMs). If a satellite successfully transmits an entangled photon pair to two ground repeaters, with each repeater in possession of one photon, the successful attempt is heralded by the repeaters' QND devices. The repeaters then store the photons in their respective QMs until they receive information about successful entanglement distribution at neighboring repeaters, at which point they may perform BSMs to extend entanglements as needed.

The more recent architecture studied in [4] allows for both ground and space repeaters. Satellites are not only fitted with entanglement sources, but also QND devices and QMs, so entanglement swapping can be executed in space as well as on Earth. Likewise, in addition to QND devices and QMs, ground stations may also be equipped with entanglement sources, so ground stations can distribute entanglement to satellites. In addition to *downlink channels*, these modifications allow for *uplink channels* and *inter-satellite links* [13].

While photon transmission in space is vulnerable to noise and loss as terrestrial photon transmission is, we shift our attention to the celestial so as to align ourselves with the most probable future direction in quantum communications [9, 13]. Indeed, the relentless stream of advances in hardware for photon transmission primes our research in the affirmative direction. The entanglement distribution problem we study is in the vein of [3, 8, 11, 12], but tailored for satellite-based quantum networks in that we distribute ebits to a pair of ground stations purely by way of LEO satellites. This reduced reliance on terrestrial channels is favorable for cross-continent entanglement distribution, an irrefutable requirement for a global quantum information network.

A study of satellite-based entanglement distribution faithful to real life would take into account factors such as the probabilistic nature of entanglement generation and swapping [2],

Alena Chang, Guoliang Xue, and Arunabha Sen are affiliated with School of Computing and Augmented Intelligence, Arizona State University, Tempe, AZ 85287. Emails: {ahchang, xue, asen}@asu.edu. Yinxin Wan is affiliated with Department of Computer Science, University of Massachusetts, Boston, MA 02125. Email: yinxin.wan@umb.edu. Alena Chang and Yinxin Wan made equal contributions to this paper. This research was supported in part by NSF grants 2007083, 2007469, and 1663651, and by the PiQPsi project of Advanced Scientific Computing Research program, U.S. Department of Energy under FWP No. ERKJ432. The information reported herein does not reflect the position or the policy of the funding agencies.

as well as entanglement fidelity [8]. However, existing studies on satellite-based entanglement distribution from a networking standpoint often do not consider satellite movement over time and/or do not permit entanglement distribution along inter-satellite links. As such, a theoretical study of a satellite-based quantum network at scale focusing on the two aforementioned factors alone is worthy of discussion.

A satellite may be within communication range of a ground station or another satellite for them to share an entangled photon pair at one point in time, but they may be too far away from each other at a different point in time. A system model studying LEO satellite-based entanglement distribution should factor in the limitations on feasible photon transmission imposed by satellite movement. However, this has not been well investigated from a networking perspective.

LEO satellite-based entanglement distribution which excludes inter-satellite links poses a major hindrance due to the fact that the communication range of a single LEO satellite, given its low altitude, cannot accommodate two ground stations whose distance exceeds the communication range. If a ground station in New York City (NYC) and a ground station in Singapore request an ebit, a single LEO satellite cannot honor their request.

Prior networking papers on satellite-based entanglement distribution include [6, 10, 15]. The system model defined in [6] lays fundamental groundwork for modeling satellite-based entanglement distribution, taking into account satellite movement over time. However, the model only considers downlinks and does not permit inter-satellite links. Similarly, [10] only considers the double downlink configuration and also does not account for satellite movement. While [15] enables inter-satellite links and considers satellite movement, it focuses on a specific scenario consisting of three satellites connecting two ground stations, in which the central satellite is positioned halfway between the ground stations. Our work addresses the following two deficits in the literature: existing at-scale models do not account for (1) satellite movement over time and (2) inter-satellite links.

To the best of our knowledge, we are the first to investigate satellite-based entanglement distribution from a networking perspective at scale while taking into account satellite movement over time and inter-satellite links. The contributions of this paper are fourfold:

- We propose a system model of an LEO satellite-based quantum network which factors in both satellite movement over time and inter-satellite links, under which we define the optimal entanglement distribution (OED) problem.
- We introduce the concept of logical graphs and demonstrate how to construct the *static* logical graph corresponding to a set of connection requests in a *dynamic* physical network.
- We design a polynomial time greedy algorithm for solving the OED problem.
- We conduct extensive performance evaluation to demonstrate the advantage of our model and algorithms.

The remainder of this paper is organized as follows. In Section 2, we define the system model and the OED problem. In Section 3, we describe the concept of logical graphs as a means to solve the OED problem. In Section 4, we present our algorithms for the OED problem. In Section 5, we present evaluation results together with our observations and analysis. In Section 6, we conclude the paper and describe directions for future research opportunities.

## 2. System Model

In this section, we present the system model for the space-ground integrated quantum network. We also formulate the entanglement distribution problem to be studied.

### A. Ground Stations and Moving Satellites

There are $R$ equally spaced rings of satellites, and each ring passes over the North and South Poles in an arrangement known as a polar orbit. Each ring contains $K$ evenly spaced satellites. The satellites are arranged so that they do not collide at the Poles. This kind of satellite constellation, known as a Walker Star constellation, has been adopted in space-based entanglement distribution work such as [6]. Different from existing models [10, 15], we offer an at-scale model taking into consideration the movement of satellites. Consequently, the geolocation of a satellite dynamically changes and is determined by time, denoted by $\tau$, where $\tau = 0$ means midnight, $\tau = 1$ means 1:00AM, etc. In contrast, the geolocation of a ground station is considered stationary. Fig. 1 illustrates an example of the type of network we study, with $R = 6$ and $K = 8$. In the figure, 28 satellites and 6 ground stations are visible, while there are a total of 48 satellites.

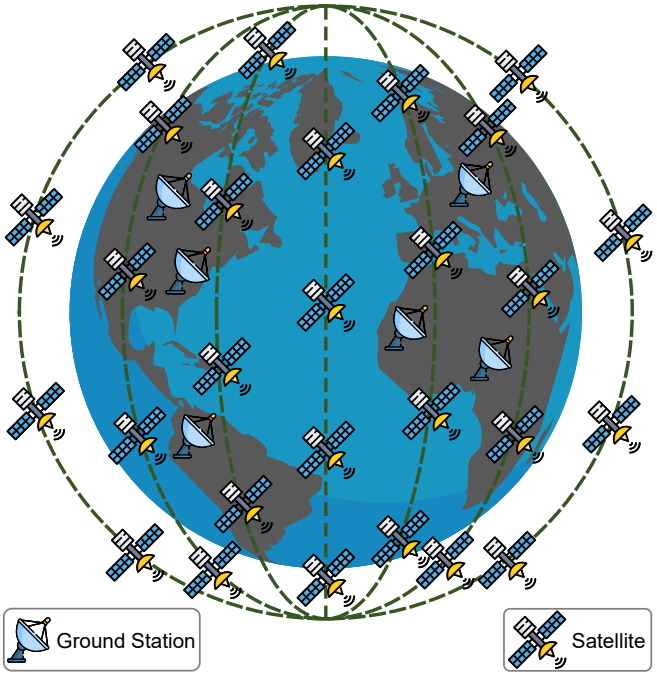


Fig. 1: An example of the type of network we study with $R = 6$ and $K = 8$.

Equipped with transmitters, receivers, and QMs, a satellite and another satellite or a ground station can establish a link if they are within each other's communication range. This distinguishes our model from existing models [6, 10] in that we allow inter-satellite links.

### B. Problem Formulation

A connection request $r_i$ is specified by a 4-tuple $(s_i, t_i, d_i, w_i)$, where $s_i$ is the *source* node which corresponds to a ground station, $t_i$ is the *destination* node which corresponds to another ground station, $d_i > 0$ is the *demand* for this connection request which quantifies the number of ebits to be transmitted, and $w_i$ is the *weight* for this connection request. To serve connection request $r_i$, we need to find an $s_i$-$t_i$ path $\pi_i$ of bandwidth $d_i$ via one or more satellites where all the satellites as well as $s_i$ and $t_i$ have sufficient transmitters, receivers, and QMs to support such an entanglement path of bandwidth $d_i$. If such a path does not exist, request $r_i$ cannot be served. If such a path exists, then the transmitters, receivers, QMs, and channels corresponding to $\pi_i$ need to be reserved for $r_i$ and must not be shared with any other connection request.

We assume that connection requests come in and are served in batches. Let $\mathcal{R} = \{r_1, r_2, \ldots, r_N\}$ be a given set of connection requests and $[\tau, \tau + \delta]$ be the time interval in which the communication links used in the entanglement paths should remain operational. The interval length $\delta > 0$ allows for as many entanglement generation and swapping attempts as needed until two nodes share an ebit. Let $\mathcal{R}'$ be a subset of $\mathcal{R}$. We say $\mathcal{R}'$ is *feasible*, if we can find a path $\pi_i$ to serve $r_i$ for each $r_i \in \mathcal{R}'$ such that (1) all of the links used in the paths are operational in the entire time interval $[\tau, \tau + \delta]$, and (2) for any two requests $r_i \in \mathcal{R}'$ and $r_j \in \mathcal{R}'$, path $\pi_i$ and path $\pi_j$ do not share any transmitters/receivers/QMs/channels. The (total) weight of $\mathcal{R}'$ is $w(\mathcal{R}') = \sum_{r_i \in \mathcal{R}'} w_i$.

The **Optimal Entanglement Distribution** (OED) problem seeks to find a feasible subset $\mathcal{R}_{opt}$ of $\mathcal{R}$ with maximum total weight. In other words, $\mathcal{R}_{opt} \subseteq \mathcal{R}$ is feasible and $w(\mathcal{R}_{opt})$ is at least as large as $w(\mathcal{R}')$ for any $\mathcal{R}' \subseteq \mathcal{R}$ that is feasible.

The introduction of weights makes the problem more general. In the unweighted case, i.e., $w_i = 1$ for all $i$, the OED problem simply seeks a feasible subset $\mathcal{R}_{opt}$ of $\mathcal{R}$ with maximum cardinality.

## 3. The Logical Graph

The OED problem involves establishing entanglements using links between two nodes whose distance changes over time (due to the movement of the satellites) and the links used are guaranteed to be operational in the entire time interval $[\tau,\tau+\delta]$. Therefore, we are dealing with a network that is *dynamic*, in the sense that a link between two nodes may exist at one time, and may not exist at another time. As a means to solve the OED problem in a dynamic network, we introduce the notion of a logical graph corresponding to a given set of connection requests $\mathcal{R}$ in the following. Therefore we will have a *physical network* that is dynamic, and a *logical graph* that is static.

Assume that the set of connection requests $\mathcal{R}$ is given. We construct a logical graph $G = (V, E)$ for $\mathcal{R}$ as follows. For each node $z$ (a satellite or a ground station) in the physical network, there is a corresponding vertex $l(z)$ in the logical graph. We use the notation $l(z)$ to mean that *node* $z$ in the physical network corresponds to *vertex* $l(z)$ in the logical graph. For each vertex $v$ in the logical graph, we use $p(v)$ to denote the corresponding node in the physical network. In other words, $l(\cdot)$ is a one-to-one mapping from the set of nodes in the physical network to the set of vertices in the logical graph; $p(\cdot)$ is a one-to-one mapping from the set of vertices in the logical graph to the set of nodes in the physical network.

For two vertices $u$ and $v$ in $V$, there is an undirected edge $(u, v) \in E$ if and only if $p(u)$ and $p(v)$ are within their communication range in the entire time interval $[\tau, \tau + \delta]$. For any given time $\tau$, we know the coordinates of $p(u)$ and the coordinates of $p(v)$. There is an edge $(u, v) \in E$ if and only if the *maximum distance between* $p(u)$ *and* $p(v)$ *in the interval* $[\tau, \tau + \delta]$ is within the communication range of $p(u)$ and $p(v)$.

If $(u, v) \in E$ is an edge, we know that $p(u)$ and $p(v)$ are within their communication range in the entire interval $[\tau, \tau + \delta]$. The *bandwidth* of edge $(u, v)$ is the number of available channels between $p(u)$ and $p(v)$. The number of transmitters/receivers/QMs at vertex $v \in V$ is the same as that in $p(v)$.

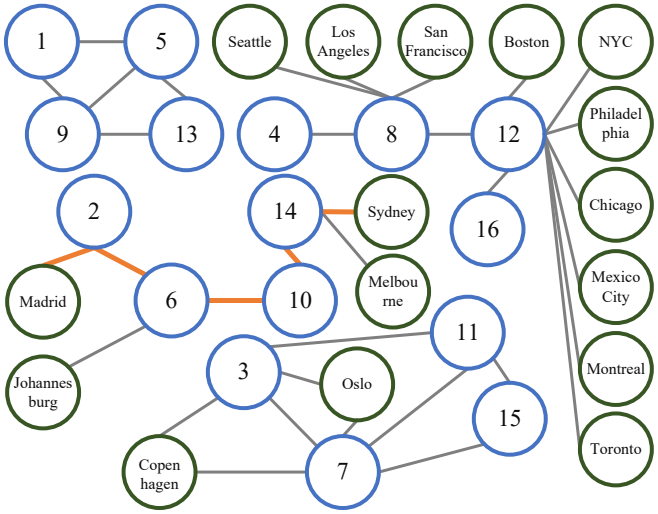


Fig. 2: An example of a logical graph where $R = K = 4$.

Fig. 2 illustrates a part of a logical graph computed a physical network where $R = K = 4$, $\tau = 1$, and $\delta = 0.01$. There are a total of 60 ground stations in the physical network, all residing in major cities across the world. In the computed logical graph, 31 ground stations have edges connecting them to satellites. To enhance readability, we only show 16 ground stations while omitting 15 which are all in Europe, and connected to satellites $S_3$ and $S_7$. There are 16 edges in the logical graph where both constituent vertices correspond to satellites in the physical network. These edges correspond to inter-satellite links in the physical network. We observe that it is possible to establish an entanglement between the ground station in Madrid and the ground station in Sydney using the path Madrid-$S_2$-$S_6$-$S_{10}$-$S_{14}$-Sydney, highlighted in Fig. 2. Such a connection is impossible without using inter-satellite links.

From the definition of the logical graph, we have the following intuitive fact whose proof is straightforward and hence omitted.

**Remark 1:** There is a $u$-$v$ path in the logical graph $G$ with bandwidth $d$ if and only if there is a physical path connecting $p(u)$ and $p(v)$ in the physical network, with bandwidth $d$, in

the entire time interval $[\tau, \tau + \delta]$. □

We should note that the logical graph is dependent on the physical network, the set of connection requests $\mathcal{R}$, and the time interval $[\tau, \tau + \delta]$.

It is worth noting that transforming dynamic satellite systems into static systems to simplify routing has been studied before. In [5], the concepts of *logical topology* and *logical node* for LEO satellite networks are introduced. However, there is a significant difference between the *logical graph* in our paper and the *logical topology* in [5]. In our paper, there is a one-to-one mapping between the set of logical nodes and the union of the satellites and the ground stations. This is not the case in the logical topology in [5]. In our paper, there is *a single logical graph corresponding to the physical system*. A logical node does not have a physical location. It has a logical mapping to a (physical) satellite or a (physical) ground station. This mapping remains the same throughout the process. In contrast, in [5], *the physical system is mapped to a set of logical topologies.* A logical node has a physical location in the orbit. A logical node in [5] corresponds to different satellites at different times. In line with the work of [5], [7] defines a temporal netgrid model which partitions the space underlying an individual satellite's orbit into netgrids to locate the satellite based on the time slot for which it occupies a netgrid. Similar to [5], [7] uses a set of static topologies, rather than a single static topology. Our approach concentrates on the worst-case guarantee, while [5] and [7] provide approximations.

Neither [5] nor [7] accommodates entanglement distribution, in which both satellites and ground stations are equipped with hardware resources which limit the number of ebits they can simultaneously generate and distribute. This constraint makes existing satellite network routing algorithms insufficient for the demands of a global quantum information network, a deficit in the literature we address.

## 4. Algorithms for OED

In Section 4-A, we present a polynomial time greedy algorithm. In Section 4-B, we present an integer linear programming (ILP)-based approach for computing an optimal solution to OED. In Section 4-C, we discuss a variant of the ILP that can be used to compute optimal entanglement distribution without using inter-satellite links.

### A. Polynomial Time Greedy Algorithm

Our greedy algorithm is presented in the following.

```
1 Sort the set of requests in non-increasing
    order based on weight/demand ratio;
2 Construct logical graph from the physical
    network and connection requests;
3 Compute a path for the request with the
    largest weight/demand ratio;
4 If there is a path satisfying this request,
    add this path to the output and update
    graph G to its residual graph;
5 Remove the request; if the request set is
    empty, stop; otherwise, go to step 3.
```

**Algorithm 1: OED-Greedy**

Our greedy algorithm considers the requests in non-increasing order of the weight-demand ratio. Whenever a request can be served, network resources are reserved for the corresponding connection request.

Algorithm 1 has an $O(N \log N + N(RK + M)^2)$ time complexity. After sorting the $N$ requests in $O(N \log N)$ time, the main steps of the algorithm consist of $N$ path finding processes, each of which can be accomplished via breadth-first-search in $O((RK + M)^2)$ time. While this algorithm does not guarantee to find an optimal solution, it is very fast, and can find close to optimal solutions in most cases, as demonstrated in our evaluations.

### B. ILP-based Optimal Algorithm

To evaluate the performance of Algorithm 1, we design an ILP-based algorithm. The main idea of our algorithm is based on integer multi-commodity flows. We associate with each request a unique commodity whose source and destination correspond to the source and destination of the request. The flow value for each commodity is either 1 (served) or 0 (not served). For each edge $(u, v) \in E$, we associate $N$ pairs of binary variables, denoting the amount of flow for commodity-$i$ from $u$ to $v$, and from $v$ to $u$, respectively. The ILP maximizes the weighted sum of flows for all commodities, subject to linear constraints described as follows. *Flow out of a source node*: For each $i \in \{1, 2, \ldots, N\}$, the net flow of type-$i$ out of source $l(s_i)$ is equal to the flow of this commodity. *Flow into a destination node*: For each $i \in \{1, 2, \ldots, N\}$, the net flow of type-$i$ into destination $l(t_i)$ is equal to the flow of this commodity. *Flow conservation*: For each $i \in \{1, 2, \ldots, N\}$, for each vertex $z \in V$ that does not correspond to $s_i$ or $t_i$, the net flow of type-$i$ into vertex $z$ is 0. *Channel capacity*: For each edge $(u, v) \in E$, the sum of all demand-flow products does not exceed the number of available channels between nodes $p(u)$ and $p(v)$. *Transmitters/Receivers/QMs*: If the flow of type-$i$ on edge $(u, v)$ is 1, we need to reserve $d_i$ transmitters at node $p(u)$, $d_i$ receivers at node $p(v)$, and $d_i$ QMs at both $p(u)$ and $p(v)$.

After solving the ILP described above, we can obtain an optimal solution to the OED problem. The optimal set of requests to be served is given by $\mathcal{R}_{opt} = \{r_i \in \mathcal{R} | \text{flow of type-}i \text{ is } 1\}$. The path $\pi_i$ for $r_i \in \mathcal{R}_{opt}$ can be obtained by tracing out the edges $(u, v)$ on which the flow of type-$i$ is 1.

### C. Restricted ILP for Systems without Inter-satellite Links

To study the impact of allowing inter-satellite links in path computation, we also design a restricted ILP-based algorithm. The restricted ILP is a slight modification of the ILP studied in Section 4-B. The only modification is not allowing inter-satellite links.

## 5. Performance Evaluation

In this section, we present the evaluation results of our space-ground integrated quantum network model as well as our proposed algorithms. The evaluation was done on a workstation running Ubuntu 22.04 system with i9-12900 CPU and 64GB memory. ILP instances were solved using the Gurobi optimizer.

### A. Evaluation Settings

**Physical Network**: We use 60 ground stations, each located in a major city in the world. Each physical network used in our evaluation consists of these 60 ground stations and $R \times K$ satellites, with $R = K$ taking a value in the set $\{1, 2, \ldots, 25\}$. We set $R$ and $K$ to be the same so that the satellites are evenly distributed around the Earth. We set the altitude of the satellites as 550km and the orbital period as 1.5 hours, both of which are consistent with LEO satellites such as Micius from the QUESS (Quantum Experiments at Space Scale) project [9, 13]. In our evaluation, we use the line-of-sight to determine the communication range. As a result, the inter-satellite communication range is 4988.11km, and the communication range between a satellite and a ground station is 2703.81km. We assume the number of transmitters, receivers, and QMs at a node to be 10. The number of available channels between two nodes within their communication range is an integer between 1 and 5.

**Connection Requests**: The source and destination nodes comprising each connection request are chosen from the pool of 60 ground stations. The demand and weight for each connection request are integers between 1 and 5. We used $N = 1, 10, 20$, and 30 in our evaluations. Start time $\tau$ takes a value in the set $\{0.0, 0.5, 1.0, 1.5, \ldots, 23.5\}$. We will describe the choice of $\delta$ in Section 5-B.

### B. Evaluation Scenarios

We evaluate our model and algorithms in the following three scenarios:

(i) In this scenario, $\mathcal{R}$ consists of one connection request, between NYC and Singapore. The demand is 1 and the weight is 1. The start time is midnight. We study two cases. In the first case, we hold $R = K$ at 10 and 20, respectively, and let $\delta$ vary from 0.00 to 0.30 in increments of 0.01. In the second case, we hold $\delta$ at 0 and 0.1, respectively, and let $R = K$ vary from 1 to 25 in increments of 1. This scenario is designed to study the impact of allowing inter-satellite links on connecting two remote ground stations. In the first case, we study the impact of $\delta$ (for fixed $R$ and $K$). In the second case, we study the impact of $R$ and $K$ (for fixed $\delta$).

(ii) In this scenario, $\mathcal{R}$ consists of 20 connection requests, with the source and destination randomly chosen from the pool of 60 ground stations. The demand and weight for each request are random integers between 1 and 5. The start time is midnight for all 20 connection requests. We study two cases. In the first case, we hold $R = K$ at 10 and 20, respectively, and allow $\delta$ to vary from 0.00 to 0.30 in increments of 0.01. In the second case, we hold $\delta$ at 0.01 and 0.1, respectively, and let $R = K$ vary from 1 to 20 in increments of 1. This scenario is designed to study the impact of $\delta$ (for fixed $R$ and $K$) and the impact of $R$ and $K$ (for fixed $\delta$), in terms of total weight.

(iii) In this scenario, for each value of $N = 10, 20$, and 30, we generate 48 different sets of connection requests: $\mathcal{R}_1^N, \mathcal{R}_2^N, \ldots, \mathcal{R}_{48}^N$. Each $\mathcal{R}_j^N$ consists of $N$ connection requests where the source and destination are randomly chosen from the 60 ground stations, and the demand and weight are random integers between 1 and 5. All connection requests in $\mathcal{R}_j^N$ have start time $0.5 \times (j-1)$. For each of $R = K = 10, 15$, and 20, we evaluate the algorithms for each of $\delta = 0.1, 0.05, 0.01$, and 0.001. This scenario is designed to conduct a more extensive performance evaluation of the proposed algorithms, with the start times evenly distributed throughout the day.

### C. Evaluation Results

In this section, we present evaluation results, together with our observations and analysis. We use `Greedy`, `ILP`, and `rILP` to denote the greedy algorithm, the ILP-based algorithm, and the restricted ILP-based algorithm, respectively.

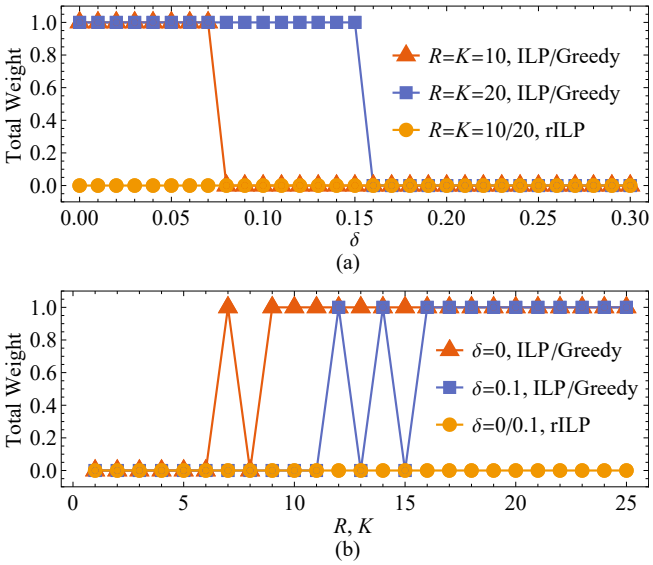


Fig. 3: Evaluation results of `Greedy`, `ILP`, and `rILP` with varying $R$, $K$, and $\delta$ for a single NYC-Singapore request with demand 1 and weight 1.

**Scenario (i):** Fig. 3 illustrates the results of Scenario (i). Fig. 3(a) shows that `Greedy` (and `ILP`) can find an NYC-Singapore path for $\delta \leq 0.07$ when $R = K = 10$, and for $\delta \leq 0.15$ when $R = K = 20$. In contrast, `rILP` cannot find such a path for any $\delta = 0.00, 0.01, \ldots, 0.30$ when both $R = K = 10$ and $R = K = 20$. This is because no single satellite can have a communication link with NYC and a communication link with Singapore at the same time.

Fig. 3(b) shows the result when we vary the value of $R = K$, with $\delta$ fixed. For $\delta = 0$, when $R = K \leq 6$, none of the algorithms can find an NYC-Singapore path. When $R = K \geq 9$, both `Greedy` and `ILP` can find an NYC-Singapore path. For $\delta = 0.1$, when $R = K \leq 11$, none of the algorithms can find an NYC-Singapore path. When $R = K \geq 16$, both `Greedy` and `ILP` can find an NYC-Singapore path.

Intuitively, when $R$ and $K$ increase, the number of edges in the logical graph also increases. But this is not always true. Hence we see the fluctuations in the figure. For $\delta = 0$, `ILP` has a weight value of 1 with $R = K = 7$, but the weight value drops to 0 when $R = K = 8$. An interesting observation is that, for a fixed time interval $[\tau, \tau + \delta]$, the total weight

corresponding to ILP is non-decreasing when $R$ (and $K$) is increased to $n \times R$ (and $m \times K$) for any integers $n \geq 1$ and $m \geq 1$. This is because the resulting logical graph is a super-graph of the original logical graph when $R$ (and $K$) is increased to $n \times R$ (and $m \times K$). For $\delta = 0$, ILP has a weight value of 1 with $R = K = 7$. When $R$ and $K$ are increased to 14 (a multiple of 7), the weight does not decrease.

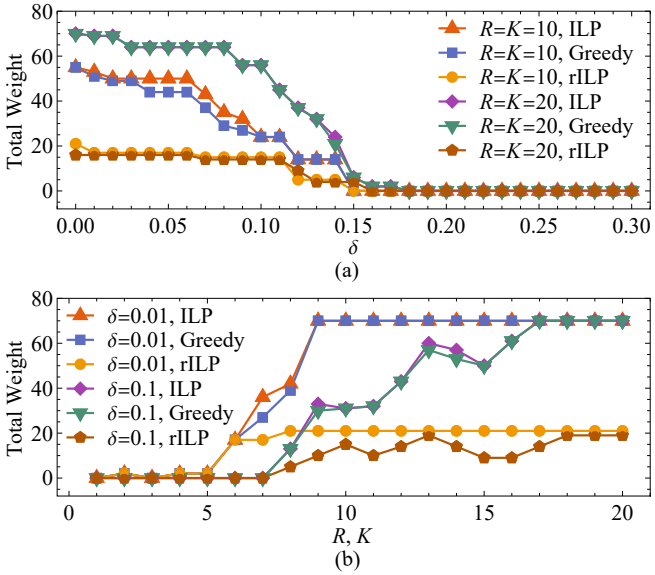


Fig. 4: Evaluations results of Greedy, ILP, and rILP with varying $R$, $K$, and $\delta$ for 20 randomly generated requests.

**Scenario (ii):** Fig. 4 illustrates the results of Scenario (ii). Fig. 4(a) shows the impact of $\delta$ on the total weight for each algorithm, with everything else fixed. We observe that the total weight is non-decreasing as $\delta$ increases. This is because fewer links will remain operational in the time interval $[\tau, \tau + \delta]$ when $\delta$ increases.

Fig. 4(b) shows the impact of $R$ (and $K$) on the total weight for each algorithm, with $\delta$ fixed. We observe that the total weight is non-decreasing (with some fluctuations) as $\delta$ increases. As explained in Scenario (i), the total weight will be non-decreasing when $R$ (and $K$) is increased to a multiple of $R$ (and $K$). Therefore, fluctuations are possible.

**Scenario (iii):** Table 1 presents more extensive evaluation results. Unlike Scenarios (i) and (ii), we have connection requests with start time $\tau$ taking the values $0.5 \times (j-1)$ for $j = 1, 2, \ldots, 48$. This means we have starting times at every hour and every half hour.

Since the test cases have different time intervals, it is less meaningful to compute the total weight across all test cases. Rather, for each test case, we compute the ratio of the weight for Greedy over that for ILP, as well as the ratio of the weight for rILP over that for ILP, and take the average of these ratios. We also record the average running times for Greedy and ILP (the running time for rILP is similar to that for ILP). We observe that Greedy requires much less time than ILP, while computing solutions nearly as good as those computed by ILP.

| $N$ | $R, K$ | $\delta$ | rILP Ratio | Greedy Ratio | Greedy Time | ILP Time |
|---|---|---|---|---|---|---|
| **10** | 10 | 0.1 | 0.1199 | 0.9966 | 0.0005$s$ | 0.1462$s$ |
| | | 0.05 | 0.1359 | 0.9831 | 0.0006$s$ | 0.1600$s$ |
| | | 0.01 | 0.1749 | 0.9982 | 0.0006$s$ | 0.1733$s$ |
| | | 0.001 | 0.1809 | 0.9990 | 0.0006$s$ | 0.1789$s$ |
| | 15 | 0.1 | 0.0915 | 0.9860 | 0.0018$s$ | 0.6498$s$ |
| | | 0.05 | 0.1803 | 1.0000 | 0.0021$s$ | 0.7640$s$ |
| | | 0.01 | 0.2210 | 1.0000 | 0.0024$s$ | 0.8754$s$ |
| | | 0.001 | 0.2272 | 1.0000 | 0.0024$s$ | 0.8875$s$ |
| | 20 | 0.1 | 0.1059 | 1.0000 | 0.0077$s$ | 3.5907$s$ |
| | | 0.05 | 0.1945 | 1.0000 | 0.0089$s$ | 4.2291$s$ |
| | | 0.01 | 0.2222 | 1.0000 | 0.0098$s$ | 4.7088$s$ |
| | | 0.001 | 0.2287 | 1.0000 | 0.0101$s$ | 4.9035$s$ |
| **20** | 10 | 0.1 | 0.1393 | 0.9756 | 0.0009$s$ | 0.2715$s$ |
| | | 0.05 | 0.1329 | 0.9643 | 0.0011$s$ | 0.3185$s$ |
| | | 0.01 | 0.1606 | 0.9932 | 0.0012$s$ | 0.3430$s$ |
| | | 0.001 | 0.1700 | 0.9936 | 0.0012$s$ | 0.3519$s$ |
| | 15 | 0.1 | 0.0868 | 0.9683 | 0.0034$s$ | 1.3464$s$ |
| | | 0.05 | 0.1576 | 1.0000 | 0.0038$s$ | 1.5269$s$ |
| | | 0.01 | 0.1980 | 1.0000 | 0.0043$s$ | 1.7278$s$ |
| | | 0.001 | 0.2056 | 1.0000 | 0.0044$s$ | 1.7764$s$ |
| | 20 | 0.1 | 0.0959 | 1.0000 | 0.0146$s$ | 6.9379$s$ |
| | | 0.05 | 0.1719 | 1.0000 | 0.0168$s$ | 8.1285$s$ |
| | | 0.01 | 0.2074 | 1.0000 | 0.0186$s$ | 9.0636$s$ |
| | | 0.001 | 0.2128 | 1.0000 | 0.0191$s$ | 9.2650$s$ |
| **30** | 10 | 0.1 | 0.1618 | 0.9523 | 0.0014$s$ | 0.4592$s$ |
| | | 0.05 | 0.1296 | 0.9311 | 0.0017$s$ | 0.5930$s$ |
| | | 0.01 | 0.1517 | 0.9685 | 0.0018$s$ | 0.6046$s$ |
| | | 0.001 | 0.1569 | 0.9736 | 0.0018$s$ | 0.6210$s$ |
| | 15 | 0.1 | 0.0834 | 0.9455 | 0.0055$s$ | 2.3433$s$ |
| | | 0.05 | 0.1441 | 0.9978 | 0.0074$s$ | 2.9550$s$ |
| | | 0.01 | 0.1856 | 1.0000 | 0.0084$s$ | 3.4108$s$ |
| | | 0.001 | 0.1945 | 1.0000 | 0.0086$s$ | 3.4192$s$ |
| | 20 | 0.1 | 0.0965 | 0.9981 | 0.0215$s$ | 10.6800$s$ |
| | | 0.05 | 0.1649 | 1.0000 | 0.0247$s$ | 14.7769$s$ |
| | | 0.01 | 0.1929 | 1.0000 | 0.0274$s$ | 16.4577$s$ |
| | | 0.001 | 0.1992 | 1.0000 | 0.0281$s$ | 16.9239$s$ |

TABLE 1: Performance of Greedy, ILP, and rILP for 1728 test cases.

## 6. Conclusion and Research Opportunities

In this paper, we have proposed a system model for a space-ground integrated quantum network. Unlike previous research, we take into consideration the movement of the satellites and inter-satellite links. We also ensure that all links used in the computed entanglement paths are guaranteed to be operational within an entire time interval.

To study entanglement distribution in such a dynamic network, we propose a novel concept of logical graphs. We design a polynomial time greedy algorithm for solving the entanglement distribution problem in a dynamic physical network with the aid of the corresponding logical graph.

We demonstrate that it is possible to establish an NYC-Singapore path using inter-satellite links. Extensive evaluations show that our greedy algorithm can compute solutions that are nearly as good as optimal, while using much less time.

Open areas for future research include developing satellite-based entanglement distribution algorithms which take into account the probabilistic nature of entanglement generation and swapping. Such probabilities should factor in the various sources of noise and loss such as weather conditions. Algorithms along this avenue could also factor in entanglement fidelity and quantum memory cutoff times, which determine how long an entangled photon is stored in memory before being discarded. As the fidelity of an ebit degrades over time, cutoffs are necessary to ensure only high-quality ebits.

## REFERENCES


[1] K. Boone, J.-P. Bourgoin, E. Meyer-Scott, K. Heshami, T. Jennewein, and C. Simon, "Entanglement over global distances via quantum repeaters with satellite links," *Phys. Rev. A*, Vol. 91, no. 5, 2015.

[2] A. Chang and G. Xue, "Order matters: On the impact of swapping order on an entanglement path in a quantum network," in *Proc. of IEEE INFOCOM WKSHPS*, 2022.

[3] L. Chen, K. Xue, J. Li, R. Li, N. Yu, Q. Sun, and J. Lu, "Q-DDCA: Decentralized dynamic congestion avoid routing in large-scale quantum networks," *IEEE/ACM Trans. Netw.*, pp. 1–14, 2023.

[4] M. Gündoğan, J. S. Sidhu, V. Henderson, L. Mazzarella, J. Wolters, D. K. L. Oi, and M. Krutzik, "Proposal for space-borne quantum memories for global quantum networking," *npj Quantum Information*, vol. 7, no. 128, 2021.

[5] Y. Hu and V. Li, "Logical topology-based routing in leo constellations," in *IEEE Int. Conf. Commun.*, vol. 10, 2001, pp. 3172–3176.

[6] S. Khatri, A. J. Brady, R. A. Desporte, M. P. Bart, and J. P. Dowling, "Spooky action at a global distance: analysis of space-based entanglement distribution for the quantum internet," *npj Quantum Information*, vol. 7, no. 4, 2021.

[7] J. Li, H. Lu, K. Xue, and Y. Zhang, "Temporal netgrid model-based dynamic routing in large-scale small satellite networks," *IEEE Trans. Veh. Technol.*, vol. 68, no. 6, pp. 6009–6021, 2019.

[8] J. Li, M. Wang, K. Xue, N. Yu, Q. Sun, and J. Lu, "Fidelity-guaranteed entanglement routing in quantum networks," *IEEE Trans. Commun.*, vol. 70, no. 10, 2022.

[9] Z. Li, K. Xue, J. Li, L. Chen, R. Li, Z. Wang, N. Yu, D. S. Wei, Q. Sun, and J. Lu, "Entanglement-assisted quantum networks: Mechanics, enabling technologies, challenges, and research directions," *IEEE Commun. Surv. Tutor.*, 2023.

[10] N. K. Panigrahy, P. Dhara, D. Towsley, S. Guha, and L. Tassiulas, "Optimal entanglement distribution using satellite based quantum networks," in *Proc. of IEEE INFOCOM WKSHPS*, 2022.

[11] M. Pant, H. Krovi, D. Towsley, L. Tassiulas, L. Jiang, P. Basu, D. Englund, and S. Guha, "Routing entanglement in the quantum internet," *npj Quantum Information*, vol. 5, no. 25, 2019.

[12] S. Shi and C. Qian, "Concurrent entanglement routing for quantum networks: Model and designs," in *Proc. of ACM SIGCOMM*, 2020.

[13] J. S. Sidhu, S. K. Joshi, M. Gündoğan, T. Brougham, D. Lowndes, L. Mazzarella, M. Krutzik, S. Mohapatra, D. Dequal, G. Vallone, P. Villoresi, A. Ling, T. Jennewein, M. Mohageg, J. G. Rarity, I. Fuentes, S. Pirandola, and D. K. L. Oi, "Advances in space quantum communications," *IET Quantum Communication*, vol. 2, no. 4, pp. 182–217, 2021.

[14] R. Van Meter, *Quantum Networking*. John Wiley & Sons, 2014.

[15] J. Wallnöfer, F. Hahn, M. Gündoğan, J. S. Sidhu, F. Wiesner, N. Walk, J. Eisert, and J. Wolters, "Simulating quantum repeater strategies for multiple satellites," *Communications Physics*, vol. 5, no. 169, 2022.